

BFKL Physics in Dijet Production at the LHC

Lynne H. Orr^a and W. J. Stirling^b

^a *Department of Physics and Astronomy, University of Rochester, Rochester,
NY 14627-0171, USA*

^b *Departments of Physics and Mathematical Sciences, University of Durham, Durham,
DH1 3LE, UK*

Abstract

The production in hadron-hadron collisions of jet pairs with large rapidity separation and comparable modest transverse momentum is, in principle, described by the perturbative QCD BFKL equation. The measurement of such jet pairs appears well suited to the LHC detectors, with their ability to detect forward jets. We present predictions for dijet cross sections and correlations obtained using a BFKL Monte Carlo which allows kinematic and other subleading effects to be incorporated. The enhanced phase space for gluon emission at the LHC makes the BFKL behavior somewhat easier to observe than at the Tevatron, although kinematic effects are still important. The production of forward jets in association with heavy Higgs bosons via the gauge boson fusion mechanism is also studied and compared with QCD dijet production.

1 Introduction

In perturbative QCD physical quantities are typically computed in fixed-order expansions in powers of the coupling constant α_S . In some kinematic regimes, however, large logarithms multiply the coupling and the series must be resummed to all orders. In certain cases this resummation is possible and meaningful predictions can still be obtained. For example, large logarithms in the small- x region in deep inelastic lepton-hadron scattering are resummed by the Balitsky, Fadin, Kuraev and Lipatov (BFKL) equation [1], to yield the well-known BFKL prediction $F_2 \sim (1/x)^\lambda$, with $\lambda = 4C_A \ln 2 \alpha_S/\pi \approx 0.5$.

In hadron collisions BFKL resummation also applies to production of jet pairs at large rapidity separation Δ when the jets have comparable transverse momenta that are small compared to the center-of-mass energy. At large values of Δ , the cross section receives contributions from real and virtual gluons emitted in the rapidity interval between the two jets, as illustrated in Fig. 1(a). The BFKL equation resums the leading logarithmic contributions from these gluons [2], giving rise to a cross section that increases with Δ , $\hat{\sigma} \sim \exp(\lambda\Delta)$, with λ defined above. Mueller and Navelet [2] pointed out the potential of this increase, which does not appear in lowest-order QCD, to provide a way to investigate BFKL physics at hadron colliders by looking at dijet production at large rapidity separation.

Unfortunately the Δ increase disappears when the subprocess cross section is folded in with parton distribution functions (pdfs), which decrease with Δ more rapidly than $\hat{\sigma}$ increases. Several methods have been suggested to avoid this pdf sensitivity when studying ‘Mueller-Navelet’ jets. One [3, 4, 5] is to study the decorrelation in the two jets’ azimuthal angles that arises from emission of gluons between the jets; BFKL predicts a stronger decorrelation than does fixed-order QCD, and this prediction should be relatively insensitive to the pdfs. Another [2, 6] is to look for the Δ increase in the ratio of dijet cross sections at two center-of-mass energies for corresponding parton momentum fractions, so that the pdfs cancel.

In practice it is not useful to compare analytic asymptotic BFKL predictions directly with experiment because nonleading corrections can be large. In particular, in the analytic BFKL calculation gluons can be emitted arbitrarily, with no kinematic cost, and energy and momentum are not conserved. In Refs. [5, 6] (see also [7]) a Monte Carlo approach is used in which the emitted gluons are subject to kinematic constraints, and other nonleading effects such as the running of α_S are included. Kinematic constraints are seen to have a significant effect, suppressing the emission of large numbers of energetic gluons. The studies in [5] and [6] focused on the azimuthal decorrelation and cross section ratios at the Fermilab Tevatron $p\bar{p}$ collider.

Here we are concerned with dijet production at the CERN LHC pp collider. The phase space available for studying dijet production is larger at the LHC than at the Tevatron, because the center-of-mass energy is much higher while measurable jet transverse momentum thresholds increase only slightly, if at all. As a result we expect kinematic constraints to have weaker effects at the LHC, so that the predictions of naive BFKL should be more robust than at the Tevatron. We will address this in more detail below.

BFKL physics (or, more generically, QCD) is not the only potential source of jet pairs with large rapidity separation at the LHC: heavy Higgs production via gauge boson fusion in

the process $qq \rightarrow qqH$ (see Fig. 1(b)) is well known to give rise to forward jets [8, 9]. In fact the forward calorimetry in the LHC detectors has been designed to be able to detect jets at large rapidity for the purpose of observing this process [10]. Detection of jets with rapidity $|y| \lesssim 5$ (i.e. $\Delta \lesssim 10$) and transverse momentum $p_T > \mathcal{O}(20 \text{ GeV})$ should be possible.

In contrast to the BFKL case, where the region between the jets is populated by gluons, the jets produced in association with the Higgs are characterized by an absence of hadronic activity between them — a ‘rapidity gap.’ We will see other differences when we compare other features of dijet production in the two cases below. The Higgs process therefore acts as a useful comparator for the BFKL study.

The paper is organized as follows. In the next section we summarize the essential features of the BFKL MC calculation used to obtain our results. In section 3 we present results for dijet production in pp collisions at center-of-mass energy 14 TeV, first in the BFKL approach, and then for jets produced in association with a heavy Higgs boson. In section 4 we investigate the collision energy dependence of the BFKL dijet cross section and present the ratio of cross sections at 10 and 14 TeV. In section 5 we present our conclusions.

2 Improved BFKL approach to dijet production in hadron collisions

The differential subprocess cross section for production of a jet pair with rapidity difference $\Delta \equiv |y_1 - y_2|$ and relatively small transverse momenta p_{T1}, p_{T2} is given in the BFKL approach by

$$\frac{d\hat{\sigma}}{d^2p_{T1}d^2p_{T2}d\Delta} = \frac{\alpha_S^2 C_A^2}{p_{T1}^2 p_{T2}^2} f(\vec{p}_{T1}, \vec{p}_{T2}, \Delta). \quad (1)$$

The Laplace transform of the function f with respect to Δ satisfies the BFKL equation. This equation contains integrals over both real and virtual gluons, and when its Laplace-transformed solution is substituted into Eq. (1), it gives the sum over emitted gluons and total cross section behavior discussed above. This is the ‘naive’ BFKL case.

As indicated in the introduction, the price of having an analytic solution is integration over radiated gluons with arbitrarily large transverse energies. We can improve on this approach by unfolding the implicit sum over gluons that appears in the analytic solution. Details can be found in [5]; see also [7] for a similar approach. The basic idea is that real gluons are separated into ‘resolved’ and ‘unresolved’ gluons, the latter being those that fall below a transverse momentum threshold μ_0 and are undetectable as jets. The unresolved gluon contributions are then combined with those from virtual contributions to give an overall form factor that suppresses the cross section. The cross section is then an explicit sum over resolved real gluons; for fixed α_S it becomes

$$\frac{d\hat{\sigma}_{gg}}{d^2p_{T1}d^2p_{T2}d\Delta} = \frac{\alpha_S^2 C_A^2}{p_{T1}^2 p_{T2}^2} \left[\frac{\mu_0^2}{p_{T1}^2} \right]^{\alpha_S C_A \Delta / \pi} \sum_{n=0}^{\infty} \mathcal{R}^{(n)}(\vec{p}_{T1}, \vec{p}_{T2}, \Delta), \quad (2)$$

with $\mathcal{R}^{(0)} = \delta(\vec{p}_{T1} + \vec{p}_{T2})$ and $\mathcal{R}^{(n)}$ for $n > 0$ given in [5], where the expressions for running α_S can also be found. The analytic result for the total cross section is reproduced in the

limit $\mu_0 \rightarrow 0$.¹

It is straightforward to implement this in a Monte Carlo program where kinematic cuts can be applied directly. The total cross section is obtained by folding in the subprocess cross section (2) with the appropriate parton distributions functions; see [5] for details.

3 Jet pair production in pp collisions at $\sqrt{s} = 14$ TeV

3.1 BFKL calculation of dijet production

The results shown here were obtained using the BFKL Monte Carlo program described above and in Ref. [5]. We consider dijet production in which the jets have equal and opposite rapidity $y_1 = -y_2 = \Delta/2$ and transverse momentum greater than some value P_T .² For the LHC we consider transverse momentum thresholds $P_T = 20$ GeV and $P_T = 50$ GeV. Given the high level of hadronic activity at the LHC, the former value may be slightly optimistic but the latter is certainly achievable [10]. We use CTEQ4L parton distributions [11].

Figure 2 shows the dijet production cross section at the LHC with center-of-mass energy 14 TeV for $p_T > 20$ GeV (upper curves) and $p_T > 50$ GeV (lower curves). All of the curves fall off with increasing Δ as a result of pdf suppression; note that the difference in momentum thresholds causes the $p_T > 50$ GeV cross sections to reach the kinematic limit at smaller values of Δ than the $p_T > 20$ GeV curves.

The naive BFKL prediction, obtained using the analytic (asymptotic) BFKL solution combined with pdfs assuming lowest-order kinematics, is shown as dashed curves in the figure. For both p_T thresholds, the naive BFKL cross section is largest for all values of Δ ; this reflects the rise with Δ of the subprocess cross section. The falloff with Δ is due to the pdfs. The BFKL MC results, shown as solid curves, lie well below naive BFKL as a result of the kinematic suppression.³ Clearly nonleading effects due to kinematics are important. Also shown for comparison are the cross sections in the asymptotic (large Δ) lowest-order QCD limit (see [6] for details about this limit). It lies below the naive BFKL curves, because the subprocess cross section is asymptotically flat in Δ , and it lies above the BFKL MC curves because it reflects only leading-order kinematics, whereas the BFKL MC cross section pays the pdf penalty for emitted gluons.

A characteristic of BFKL dijets that clearly distinguishes them from those in leading-order QCD is a decorrelation in azimuthal angle at large values of Δ [3, 4, 5]. In QCD at lowest order the two jets are strictly back-to-back in the transverse plane, so that their azimuthal angles are completely correlated, independent of rapidity. In contrast, in the BFKL case gluons are radiated in the rapidity interval between the two jets, and as this interval increases more gluons can be radiated. The presence of these gluons weakens the azimuthal correlation between the two jets of interest, so that one sees an increasing azimuthal decorrelation as Δ increases.

¹In practice, the value $\mu_0 = 1$ GeV gives a very good approximation to the limiting result and acceptable Monte Carlo efficiency. In general μ_0 should be small compared to p_{T1}, p_{T2} .

²Equal and opposite rapidities are taken for convenience only and are not required for validity of the BFKL approach; the rapidity separation is the important quantity.

³The running of α_S also contributes to the suppression but kinematics is the main effect.

As discussed in [5], applying kinematic constraints as in the improved BFKL MC gives less of a decorrelation than predicted in naive BFKL because emission of arbitrarily many gluons of arbitrary energy is no longer allowed. In fact, for any given transverse momentum threshold, there is some Δ at which the jet pair alone saturates the kinematic limit, and emission of additional (real) gluons is completely suppressed and the azimuthal correlation returns. As we approach that limiting value of Δ we therefore expect to see a transition back towards correlated jets.

This is illustrated in Fig. 3, where we show the azimuthal decorrelation in dijet production in the improved BFKL MC approach (upper curves). We show the mean value of $\cos \Delta\phi$ where we have defined

$$\Delta\phi \equiv |\phi_1 - \phi_2| - \pi \quad (3)$$

so that $\Delta\phi = 0$ when the two jets are back-to-back in the transverse plane. The jets are completely correlated at $\Delta = 0$, and as Δ increases we see the characteristic BFKL decorrelation, followed by a flattening out and then an increase in $\langle \cos \Delta\phi \rangle$ as we approach the kinematic limit. Not surprisingly, the kinematic constraints have a much stronger effect when the p_T threshold is set at 50 GeV (dashed curve) than at 20 GeV (solid curve); in the latter case more phase space is available to radiate gluons. We also show for comparison the decorrelation for dijet production at the Tevatron for $p_T > 20$ GeV. There we see that the lower collision energy (1.8 TeV) limits the allowed rapidity difference and substantially suppresses the decorrelation at large Δ . The larger center-of-mass energy compared to transverse momentum threshold at the LHC would seem to give it a significant advantage as far as observing BFKL effects is concerned.

The lower set of curves in Fig. 3 refer to Higgs production and will be discussed below.

3.2 Forward jets from Higgs production via boson fusion

At the LHC, Higgs bosons can be produced in the process $qq \rightarrow qqH$, where W or Z bosons emitted by the initial state quarks annihilate to form a Higgs [8], see Fig. 1(b). This mechanism may be important for discovering a heavy $M_H \sim 1$ TeV Higgs, since the rate there is comparable to the rate from the ‘standard’ $gg \rightarrow H$ process, see for example Ref. [12]. For lighter Higgs bosons, weak boson fusion can provide a complementary method of checking that the couplings to heavy quarks and weak bosons are related in the way specified by the Standard Model.

Our interest here, however, is in the final-state quark jets accompanying the Higgs. The ability to ‘tag’ these jets [9] is necessary to suppress backgrounds, for example from $q\bar{q} \rightarrow WW, ZZ$, and $t\bar{t}$ production. It is the t -channel W and Z propagators (see Fig. 1(b)) that to a large extent determine the regions of phase space populated by the tag jets. Typically, they have $\mathcal{O}(\text{TeV})$ energies and transverse momenta less than M_W . They therefore naturally have large (roughly equal and opposite) rapidities.

Higgs production via WW and ZZ fusion therefore automatically provides a ‘BFKL-like’ dijet sample with large rapidity separation. Figure 4 shows the differential cross section $d^2\sigma^H/dy_1dy_2(y_1 = -y_2 = \Delta/2)$ as a function of Δ , for $M_H = 500$ GeV and $p_T > 20, 50$ GeV at the LHC. Notice the difference in shape compared to the QCD LO dijet distributions shown in Fig. 2; the tag jets are naturally produced with a sizeable rapidity separation.

The big difference between Higgs and QCD dijet production is of course the t -channel color *singlet* exchange property of the former. This gives rise to a rapidity *gap*, rather than a region between the jets populated by BFKL soft gluons, Fig. 1(a).⁴ The large rapidity separation decorrelation between the forward jets induced by multigluon emission between them is therefore absent. Interestingly, however, for $M_H \gg p_T(\text{jet})$ the centrally produced Higgs boson acts as a jet decorrelator, i.e. the $qq \rightarrow Hqq$ matrix element does not depend on the relative orientation of $p_{T1}^{\vec{}}$ and $p_{T2}^{\vec{}}$. Indeed the only significant correlation occurs when the tag jets are produced centrally (small Δ) and all invariants $p_i \cdot p_j$ are large and of the same order. Three-body kinematics then yields approximately back-to-back jets. The situation is summarised in Fig. 3, which shows the Δ dependence of $\langle \cos \Delta\phi \rangle$ for the $qq \rightarrow qqH$ process (lower set of curves). We have again taken $M_H = 500$ GeV, but in fact the dependence on the (heavy) Higgs mass is very weak. Evidently the jets accompanying Higgs production are much *more* decorrelated in azimuth than the Mueller-Navelet QCD jets. In principle, therefore, the Higgs tag jets could act as a benchmark for the decorrelation, since the theoretical predictions shown in Fig. 3 should be reliable.

4 Collision energy dependence of dijet production at the LHC

The BFKL increase in the dijet subprocess cross section with Δ is swamped by the decreasing parton distribution functions, as can be seen in Fig. 2. One way [2, 6] to account for this is to take a ratio of cross sections at different Δ but at the same values of parton momentum fraction x so that the pdf dependence cancels out. This requires (at least) two center-of-mass energies. The difficulty with this method, as discussed in [6], is that the cancellation of pdfs only occurs using lowest-order kinematics; like any other quantity, the cross section ratio is subject to corrections due to kinematic effects. As shown in [6], these kinematic effects turn out to be very important at the Tevatron (for $\sqrt{s} = 630$ and 1800 GeV) and the improved BFKL MC prediction differs qualitatively from that of naive BFKL.

In this section we investigate the dijet cross section ratio at the LHC, for the design center-of-mass energy $\sqrt{s} = 14$ TeV and for $\sqrt{s} = 10$ TeV, which has been mentioned as a possible first step toward the design energy. At the LHC, the higher center-of-mass energy compared to transverse momentum threshold may mitigate the strong kinematic suppression that spoiled the naive BFKL ratio at the Tevatron.

We consider a cross section ratio R_{12} at center-of-mass energies $\sqrt{s_1}$ and $\sqrt{s_2}$ measured at fixed values of rapidity difference Δ_1 and Δ_2 chosen so that the asymptotic lowest-order QCD cross sections (including pdfs) are equal [6]. Given Δ_1 , Δ_2 is given by

$$\frac{\cosh(\frac{1}{2}\Delta_1)}{\cosh(\frac{1}{2}\Delta_2)} = \frac{\sqrt{s_1}}{\sqrt{s_2}}. \quad (4)$$

⁴The existence of this rapidity gap has been suggested as an additional signature for Higgs production, see for example Ref. [13].

The cross section ratio to be measured is then

$$R_{12} = \frac{d\sigma(\sqrt{s_1}, \Delta_1)}{d\sigma(\sqrt{s_2}, \Delta_2)} \quad (5)$$

One advantage of this definition is that it uses the rapidity differences between the two outside jets, rather than the parton momentum fractions for the event, which can be more difficult to measure [14].

In Fig. 5 we show R_{12} at the LHC with $\sqrt{s_1} = 10$ TeV and $\sqrt{s_2} = 14$ TeV as a function of Δ_1 , with Δ_2 determined by Eq. (4). Note that although we show results for all values of Δ , it is really only at the larger values that we expect BFKL behavior to be manifest. In asymptotic LO QCD $R_{12} = 1$ by construction; it is shown for reference as a dotted line in the figure. We show the naive BFKL (lower curves) and improved BFKL MC (upper curves) ratios for $p_T > 50$ GeV (dashed curves) and $p_T > 20$ GeV (solid curves). As at the Tevatron, we see that the BFKL MC predictions deviate strongly from those of naive BFKL due to nonleading effects. The situation is slightly better than at the Tevatron, where the cross section was never larger at 1800 GeV than at 630 GeV, in marked contrast to the naive BFKL expectation. Again, the LHC benefits from the larger available phase space.

5 Conclusions

In summary, the ability of the LHC general purpose detectors to measure ‘Mueller-Navelet’ forward jets with large rapidity and modest transverse momentum will allow an important test of QCD ‘BFKL’ physics. In this paper we have presented the results of an improved BFKL Monte Carlo calculation for dijet production at large rapidity separation at the LHC. In this approach, subleading effects such as kinematic constraints and the running of the strong coupling constant α_S are incorporated by unfolding the implicit BFKL sum over emitted gluons to make the sum explicit.⁵

We found that, as at the Tevatron [5, 6], these subleading effects can be substantial and in particular lead to some suppression of gluon emission. This kinematic suppression is however not as dramatic at the LHC, because of its relatively higher center-of-mass energy compared to the jet transverse momentum threshold. As a result, improved BFKL MC predictions tend to retain more BFKL-type behavior because of the greater phase space for emitting gluons. We saw that as the p_T threshold was lowered, the BFKL MC results became more naive-BFKL-like. This was true for both the azimuthal decorrelation and the cross section ratio at different collision energies.

Noting that forward jets are also produced at the LHC in heavy Higgs boson production via gauge boson fusion, we compared the two dijet production mechanisms. The Higgs case is characterized by a lack of hadronic activity in the rapidity region between the two jets (the ‘rapidity gap’), in contrast to the BFKL case where the region between the jets is populated by emitted gluons which give rise to an azimuthal decorrelation of the outside jets. Interestingly, however, we found that the Higgs boson itself acts as a decorrelator and

⁵Another potentially important effect, not included in the present study, may come from the next-to-leading order perturbative corrections to the BFKL equation, which have recently been calculated [15].

the jets produced in association with a heavy Higgs show a stronger decorrelation than the BFKL jets.

The LHC holds promise for studies of dijet production in BFKL physics, and such studies will benefit from jet detection capabilities that extend far into the forward region and allow for p_T thresholds as low as possible. However, kinematic effects can still be of quantitative importance, and should therefore be incorporated in the theoretical analyses.

Acknowledgements

This work was supported in part by the U.S. Department of Energy, under grant DE-FG02-91ER40685 and by the U.S. National Science Foundation, under grant PHY-9600155.

References

- [1] L.N. Lipatov, Sov. J. Nucl. Phys. **23** (1976) 338.
E.A. Kuraev, L.N. Lipatov and V.S. Fadin, Sov. Phys. JETP **45** (1977) 199.
Ya.Ya. Balitsky and L.N. Lipatov, Sov. J. Nucl. Phys. **28** (1978) 822.
- [2] A.H. Mueller and H. Navelet, Nucl. Phys. **B282** (1987) 727.
- [3] V. Del Duca and C.R. Schmidt, Phys. Rev. **D49** (1994) 4510; Phys. Rev. **D51** (1995) 215.
V. Del Duca and C.R. Schmidt, Nucl. Phys. Proc. Suppl. **39BC** (1995) 137; preprint DESY 94-163 (1994), presented at the 6th Rencontres de Blois, Blois, France, June 1994.
- [4] W.J. Stirling, Nucl. Phys. **B423** (1994) 56.
- [5] L.H. Orr and W.J. Stirling, Phys. Rev. **D56** (1997) 5875.
- [6] L.H. Orr and W.J. Stirling, preprint hep-ph/9801304, Phys. Lett. B, in press.
- [7] C.R. Schmidt, Phys. Rev. Lett. **78** (1997) 4531.
- [8] R.N. Cahn and S. Dawson, Phys. Lett. **B136** (1984) 196.
- [9] R.N. Cahn, S.D. Ellis, R. Kleiss and W.J. Stirling, Phys. Rev. **D35** (1987) 1626.
- [10] ATLAS Technical Proposal, CERN/LHC/94-43 LHCC/P2 (December 1994).
CMS Technical Proposal, CERN/LHC/94-43 LHCC/P1 (December 1994).
- [11] CTEQ collaboration: H.L. Lai *et al.*, Phys. Rev. **D55** (1997) 1280.
- [12] R.K. Ellis, W.J. Stirling and B.R. Webber, *QCD and Collider Physics* (Cambridge University Press, Cambridge, 1996).

- [13] Yu.L. Dokshitzer, V.A. Khoze and S.I. Troyan, in Proc. 6th Int. Conf. on Physics in Collision, ed. M. Derrick (World Scientific, Singapore, 1987), p.417.
Yu.L. Dokshitzer, V.A. Khoze and S.I. Troyan, Sov. J. Nucl. Phys. **46** (1987) 712.
J. Gunion, *et al.*, Phys. Rev. **D40** (1989) 2223.
Yu.L. Dokshitzer, V.A. Khoze and T. Sjöstrand, Phys. Lett. **B274** (1992) 116.
H. Chehime, *et al.*, Phys. Lett. **B286** (1992) 397.
J.D. Bjorken, Phys. Rev. **D45** (1992) 4077; Phys. Rev. **D47** (1993) 101.
R.S. Fletcher and T. Stelzer, Phys. Rev. **D48** (1993) 5162.
V. Barger, R.J.N. Phillips and D. Zeppenfeld, Phys. Lett. **B346** (1995) 106.
T.L. Lungov and C.O. Escobar, Phys. Rev. **D53** (1996) 4857.
V.A. Khoze, A.D. Martin and M.G. Ryskin, Phys. Lett. **B401** (1997) 330.
- [14] A. Goussiou for the DØ collaboration, presented at the International Europhysics Conference on High Energy Physics, Jerusalem, August 19–26, 1997.
- [15] V.S. Fadin and L.N. Lipatov, preprint hep-ph/9802290 (1998).
M. Ciafaloni and G. Camici, Phys. Lett. **B412** (1997) 396; Erratum **B417** (1998) 390.
G. Camici and M. Ciafaloni, preprint hep-ph/9803389 (1998).

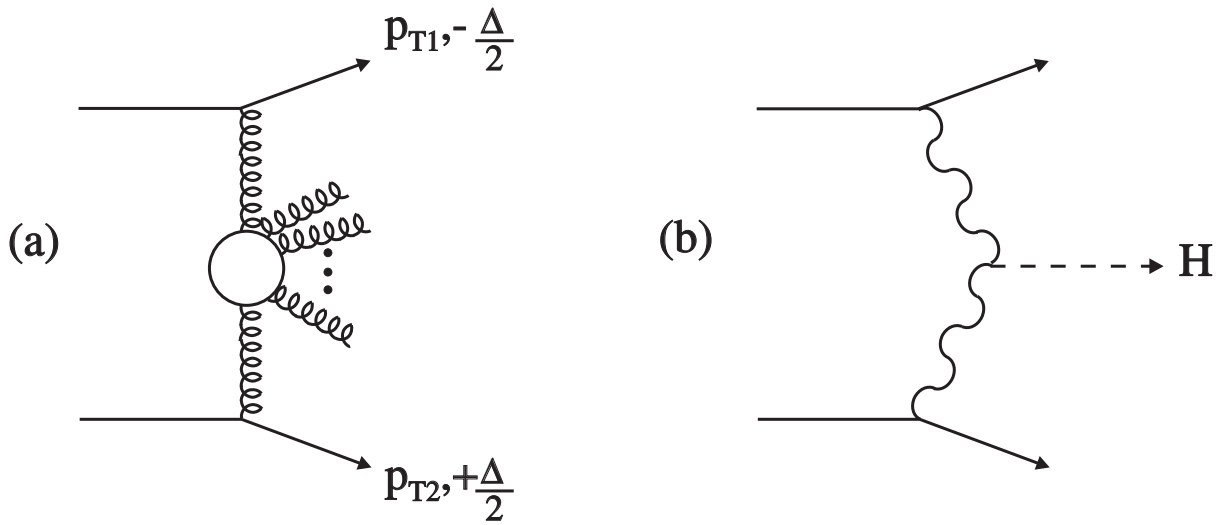


Figure 1: Schematic representation of dijet production at large rapidity separation Δ in hadron-hadron collisions in (a) the BFKL approach and (b) Higgs production via boson fusion.

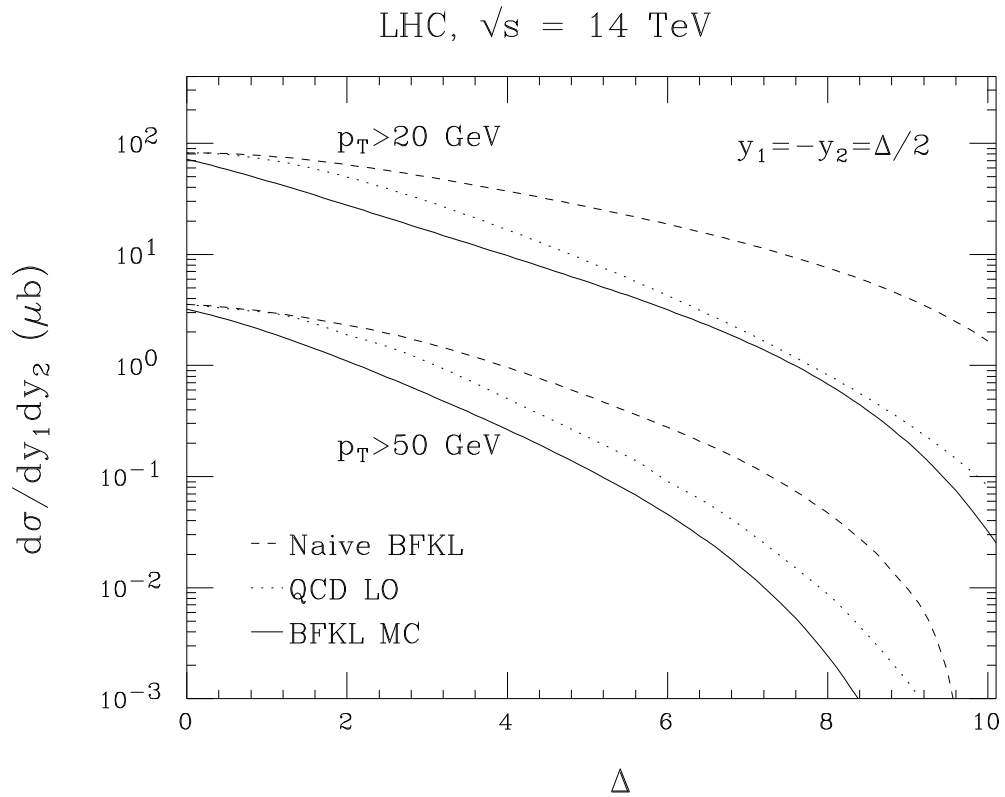


Figure 2: BFKL and asymptotic QCD leading-order dijet production cross sections at the LHC ($\sqrt{s} = 14$ TeV) as a function of the dijet rapidity separation. The pdfs are the CTEQ4L set [11]. The three curves at each transverse momentum threshold use: (i) improved BFKL MC with running α_S (solid lines), (ii) naive BFKL (dashed lines), and (iii) the asymptotic ($\Delta \gg 1$) form of QCD leading order (dotted lines).

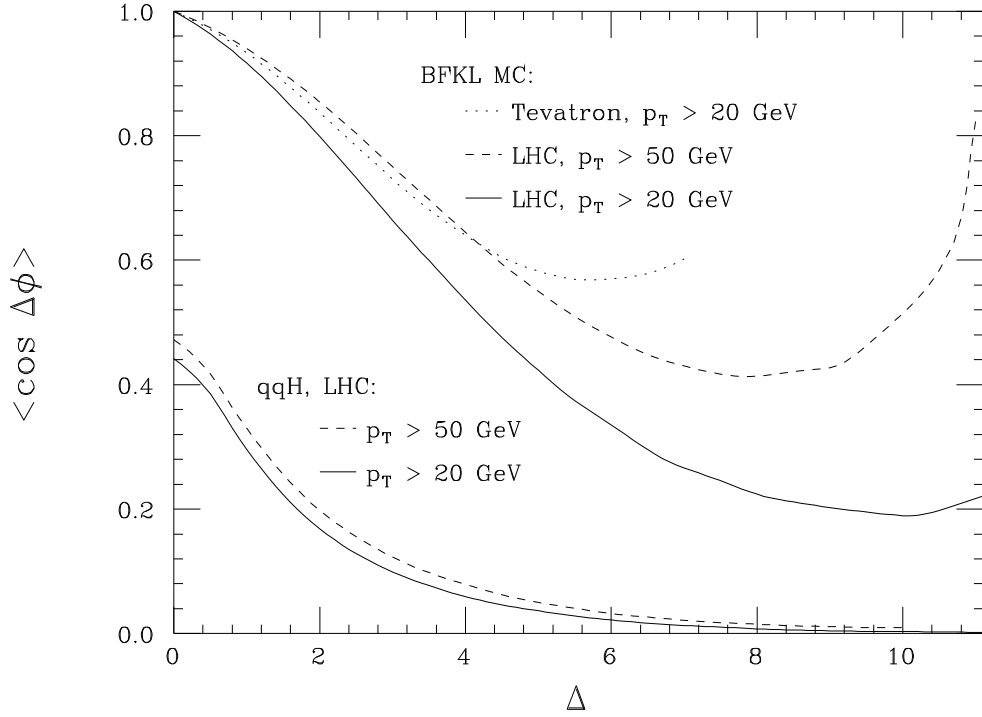


Figure 3: The azimuthal angle decorrelation in dijet production at the Tevatron ($\sqrt{s} = 1.8$ GeV) and LHC ($\sqrt{s} = 14$ TeV) as a function of dijet rapidity difference Δ . The upper curves are computed using the improved BFKL MC with running α_S ; they are: (i) Tevatron, $p_T > 20$ GeV (dotted curve), (ii) LHC, $p_T > 20$ GeV (solid curve), and (iii) LHC, $p_T > 50$ GeV (dashed curve). The lower curves are for dijet production in the process $qq \rightarrow qqH$ for $p_T > 20$ GeV (solid curve) and $p_T > 50$ GeV (dashed curve).

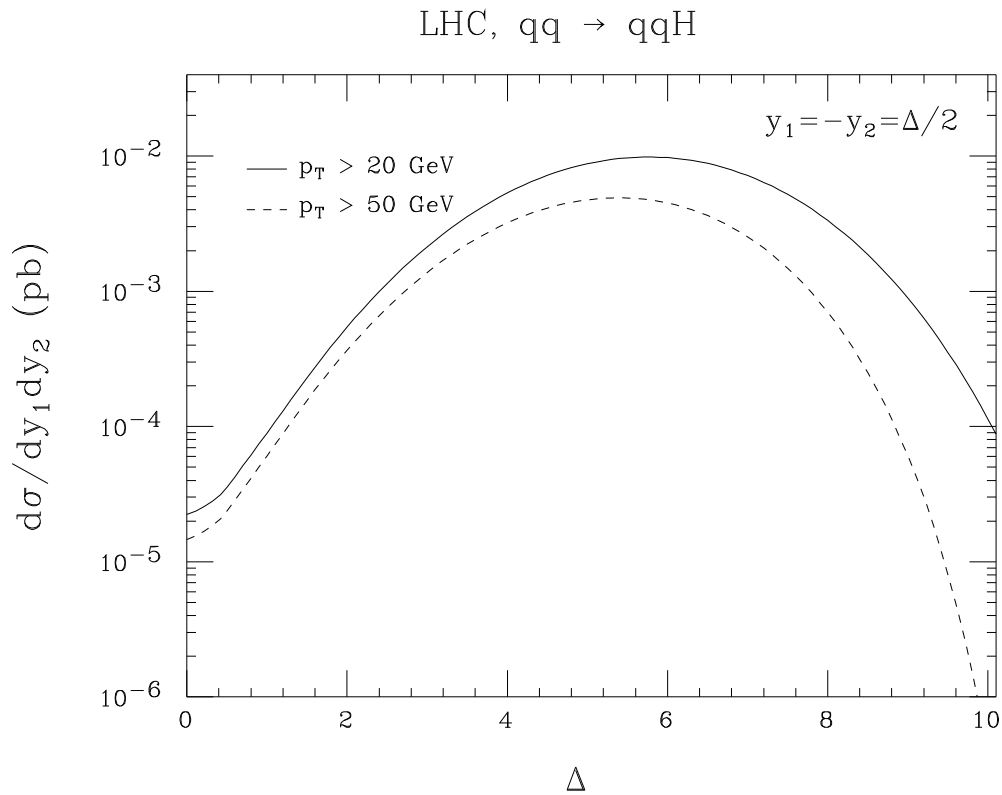


Figure 4: The cross section for the production of jet pairs in association with a Higgs boson via gauge boson fusion (Fig. 1(b)) at the LHC ($\sqrt{s} = 14$ TeV) as a function of rapidity separation of the jet pair for $p_T > 20$ GeV (solid curve), and $p_T > 50$ GeV (dashed curve). The pdfs are the CTEQ4L set [11].

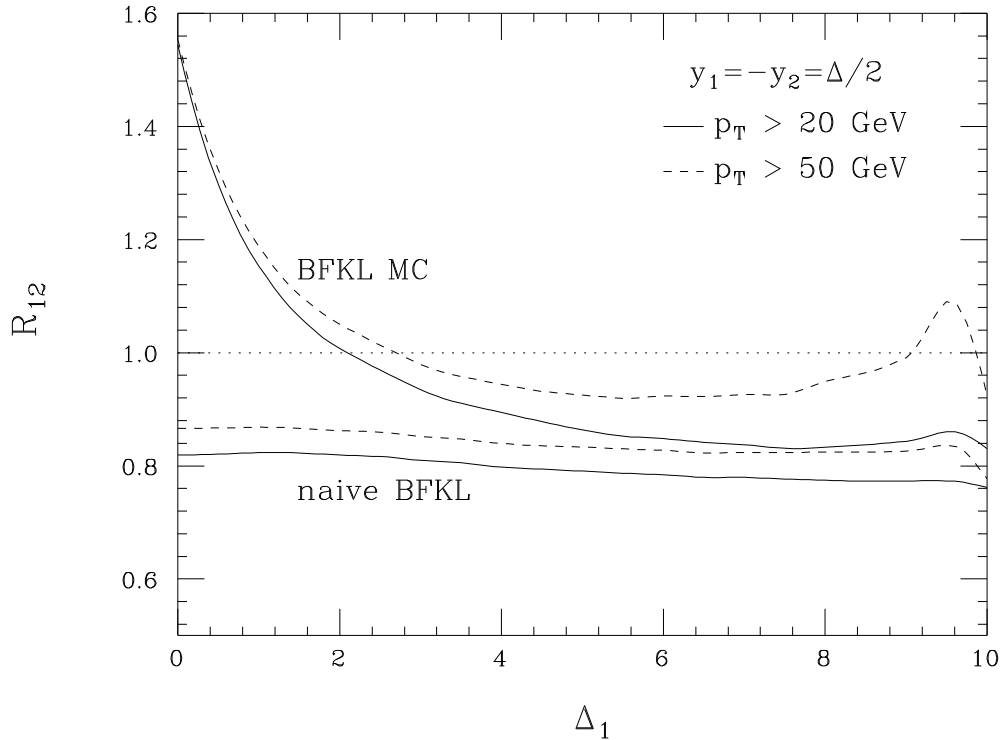


Figure 5: The ratio R_{12} of the dijet cross sections at the two collider energies $\sqrt{s_1} = 10$ TeV and $\sqrt{s_2} = 14$ TeV, as defined in the text for $p_T > 20$ GeV (solid curves), and $p_T > 50$ GeV (dashed curves). The curves are calculated according to: (i) the improved BFKL MC predictions using CTEQ4L [11] pdfs (upper curves), with $\mu = P_T = 20$ GeV, (ii) the naive BFKL prediction (lower curves), and (iii) the asymptotic leading-order prediction (dotted curve) $R_{12} = 1$.